DOI: 10.1002/ange.200802783

Membrane Proteins

# Solution-State NMR Spectroscopy of a Seven-Helix Transmembrane Protein Receptor: Backbone Assignment, Secondary Structure, and Dynamics**

*Antoine Gautier, John P. Kirkpatrick, and Daniel Nietlispach**

Solution-state NMR spectroscopy is rapidly winning importance in the study of the structure and dynamics of integral membrane proteins (IMPs). The majority of investigations concentrate on the more amenable β-barrel-type proteins.[1,2] The larger group of α-helical IMPs is more challenging to study and only a few structures of proteins with up to three helices have been determined by solution-state NMR spectroscopy, including several oligomeric structures.[3–12]

We have characterized a multispan seven-helical membrane protein receptor, sensory rhodopsin pSRII from *Natronomonas pharaonis*, using high-resolution solution NMR methods. We report the near-complete backbone assignment (>98%) of the 241-residue chain, secondary structure determination, and analysis of the backbone dynamics. Structurally, pSRII can be considered as a G protein-coupled receptor (GPCR) analogue, with the same seven-helical transmembrane architecture. The structure of pSRII has previously been solved by X-ray diffraction[13,14] and more recently this protein was also studied by solid-state NMR spectroscopy.[15] In the latter study, problems with signal overlap were partly alleviated through reverse labeling of the abundant amino acids, allowing assignment of 40% of the primary sequence.

In contrast, our approach is based on solution-state NMR spectroscopy and employs uniform $^{13}C$,$^{15}N$-labeling in combination with a high level of side-chain deuteration (>95%) to improve resolution and sensitivity. The choice of solubilizing detergent is crucial for NMR studies in solution: the native structural integrity of the protein must be preserved in the protein–detergent complex and the increase in molecular weight upon complex formation should be minimal,[16] so that adequate sensitivity is maintained to allow application of transverse relaxation-optimized spectroscopy (TROSY).[17] From a range of neutral and zwitterionic detergents tested, we found diheptanoylphospatidylcholine (DHPC) to give the best results at 50°C (Figure 1).

Flash-photolysis measurements have previously established the functionality of pSRII solubilized by dodecyl maltoside (DM).[18] The characteristic UV/Vis spectrum of pSRII resulting from the helix-embedded chromophore shows identical features in DM and DHPC solutions, and this observation together with the strong similarity between the $^{1}H$, $^{15}N$, and $^{13}Ca$ chemical shifts in the corresponding HNCA spectra indicates that the native-like structure of the protein is maintained in DHPC solution (data not shown). No detrimental changes were noticed in the UV/Vis spectrum upon increasing the temperature from 25 to 50°C, and NMR samples remained stable for over three weeks.

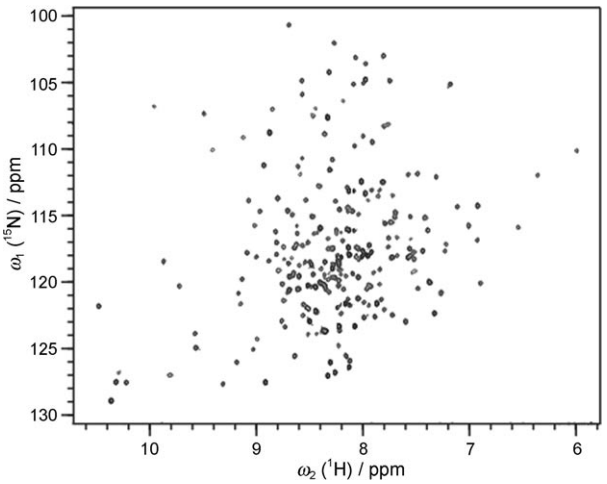


***Figure 1.*** Two-dimensional $^{1}H$–$^{15}N$ TROSY-HSQC spectrum of 0.5 mM pSRII in DHPC, at pH 5.9 and 50°C, recorded at 600 MHz. The presence of several aromatic residues in each of the seven helices improves the chemical shift dispersion.

Sequential residue assignments were obtained from six pairwise 3D out-and-back TROSY-type backbone experiments: HNCA/HN(CO)CA, HN(CA)CB/HN(COCA)CB, and HN(CA)CO/HNCO,[19,20] acquired on a uniformly $^{13}C$,$^{15}N$-labeled sample with a high level of side-chain deuteration. Critical to the success of this approach, nonuniform sampling schemes in combination with maximum entropy reconstruction were employed in all indirect chemical shift evolution periods,[21,22] maximizing the sensitivity per unit time while providing a sufficiently high spectral resolution. The sensitivity of the carbonyl experiments benefited from a lower magnetic field strength of 600 MHz, while the HNCA and HN(CA)CB experiments performed best at 800 MHz. With the exception of four residues, all non-proline residues were assigned based on $^{13}Ca$, $^{13}Cb$, and partial $^{13}C'$ shift information. The extent of the assignment is shown in Figure 2. The backbone assignments were confirmed with 3D

[*] A. Gautier, Dr. J. P. Kirkpatrick, Dr. D. Nietlispach
Department of Biochemistry, University of Cambridge
80 Tennis Court Road, Cambridge CB2 1GA (UK)
Fax: (+44) 1223-766-002
E-mail: dn206@bioc.cam.ac.uk

[**] This work was supported through the Royal Society, Marie Curie Actions (ChemBioCam), and BBSRC.

Supporting information for this article is available on the WWW under http://dx.doi.org/10.1002/anie.200802783.

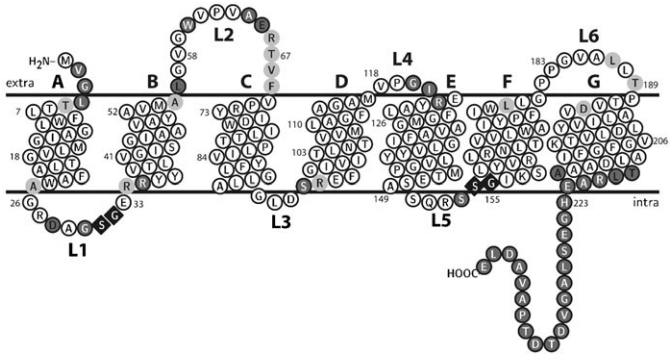


***Figure 2.*** Simplified topology diagram of pSRII showing the primary sequence with helices A–G and the loop regions L1–L6. Circles and diamonds represent assigned and unassigned residues, respectively. Amide protons shown as dark gray circles with black labels are undergoing exchange with $H_2O$ on the ms timescale (Cleanex[23]) while residues with large $^1$Hn chemical-shift/temperature coefficients ($|\Delta\delta/\Delta T| > 4.5$ ppb K$^{-1}$) are indicated in light gray with black labels. Amide protons that are subject to both phenomena are denoted by dark gray circles and white labels.

$^{15}$N-separated HNH- and NNH-NOESY experiments (200 ms mixing time) through the characteristic NOEs in the α helices between $Hn_i$ and $Hn_{i\pm k}$ ($k = 1$–3). The occurrence of NOEs between $Hn_i$ and $Hn_{i\pm1}$ also allowed verification of assignments in the loop regions and established a β-sheet stretch in L2 between residues 61–63 and 68–70. A more exhaustive use of the available NOE information would require 4D experiments to reduce signal overlap along the spectral diagonal.

Figure 3 shows the secondary-structure chemical shift information $\Delta\delta_{Ca}-\Delta\delta_{Cb}$ averaged over three successive residues.[24] The stretches of positive values clearly indicate the presence of seven helical regions A–G, which are separated by shorter stretches lacking well-defined secondary structure, most notably loops L1–L6 and the C terminus beyond residue 220. Both the $\Delta\delta_{Ca}-\Delta\delta_{Cb}$ data and the NOE pattern identify the short antiparallel β sheet in L2. A reduction of $\Delta\delta_{Ca}-\Delta\delta_{Cb}$ for Val 142 agrees with the presence of the kink in helix E preceding Gly 143 and Pro 144 seen in the crystal structure. The lengths of the individual α helices are also in agreement with the crystal structure.[13]

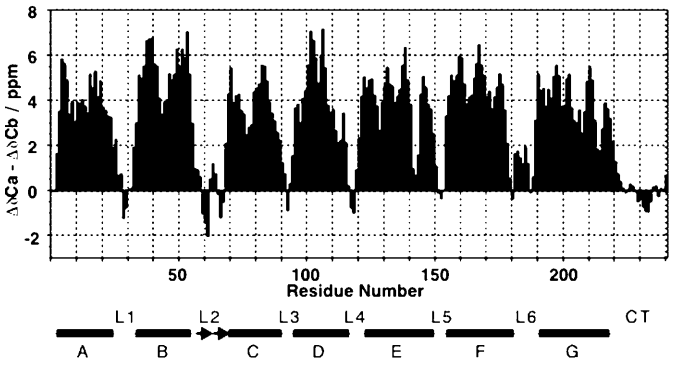


***Figure 3.*** The secondary chemical shift difference $\Delta\delta_{Ca}-\Delta\delta_{Cb}$ averaged over three successive residues plotted against the pSRII sequence; the secondary structure chart is indicated underneath.

The results of Cleanex[23] $H_2O$ exchange experiments reveal several solvent-accessible residues in loops L1, L2, and L5, and in the C-terminal region, as highlighted in Figure 2. With the exception of a few residues at the start of helices A and E, the structured residues appear not to be solvent accessible on the ms timescale probed. These identified solvent-exposed residues match well with the results of the solid-state study.[15] Changes in the hydrogen-bond network over the temperature range 25–50 °C were assessed by the $^1$Hn chemical-shift/temperature coefficient $\Delta\delta/\Delta T$. Residues with $|\Delta\delta/\Delta T|$ values larger than 4.5 ppb K$^{-1}$ were considered to undergo a significant change in their hydrogen-bonding mode[25] (see Figure 2). They are either part of solvent-exposed loop regions L1, L2, L4, L5, and L6, the C terminus, or are located towards the ends of helices A, B, D, F, and G. Large $|\Delta\delta/\Delta T|$ values were also frequently accompanied by a signal in the Cleanex experiments or an $H_2O$-exchange peak in the $^{15}$N NOESY experiments. Importantly, no changes are observed for residues that reside on the hydrophobic surface or in the buried core, indicating that the temperature increase does not induce any major structural changes.

The dynamics of pSRII were characterized through measurement of $^{15}$N $T_1$ and $T_2$ time constants, {$^1$H}–$^{15}$N heteronuclear NOEs (HNOEs) (Figure 4), and $\eta_{xy}$ cross-correlation rates. A rotational diffusion time, $\tau_c$, of 21.3 ns was determined from a trimmed $T_1/T_2$ ratio, while 20.3 ns was obtained from the $\eta/R_1$ ratio. Both correspond to a molecular weight for the protein–detergent complex of 50–70 kDa, in agreement with translational diffusion measurements; this

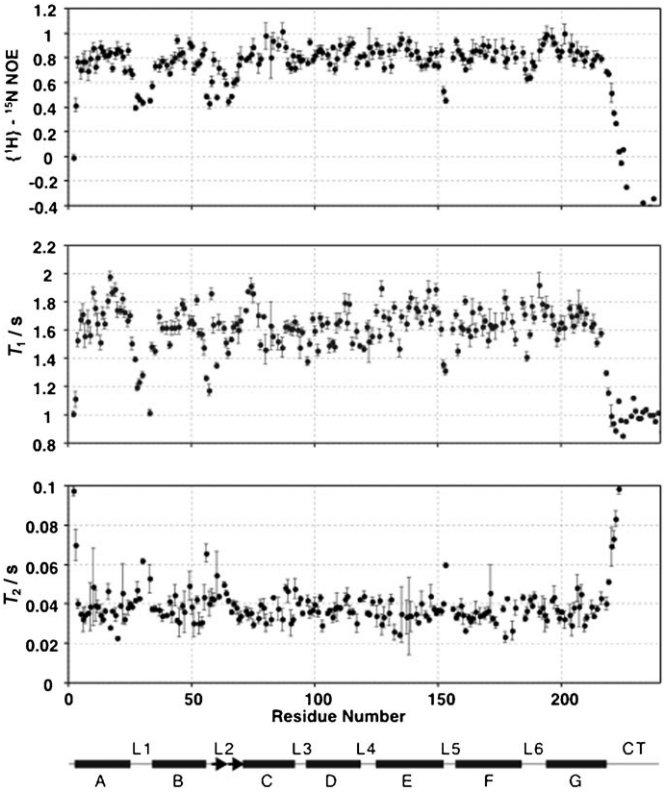


***Figure 4.*** Heteronuclear {$^1$H}–$^{15}$N NOE and $^{15}$N $T_1$ and $T_2$ relaxation data for pSRII measured at 600 MHz.

value is similar to that of previously studied porin proteins. Assuming the hydrophobic protein surface is surrounded by a torus-like DHPC layer, the complex is expected to have an oblate rotational diffusion tensor ($D_{\parallel}/D_{\perp} \approx 1.3$). With the major diffusion tensor axes perpendicular to the helix axes this would lead to an underestimation of the rotational correlation time from the $T_1/T_2$ ratio.

Helices A–G are well ordered, but some of the loop regions show varying degrees of mobility on different timescales, as shown in Figure 5a. In particular, loops L1, L2, and

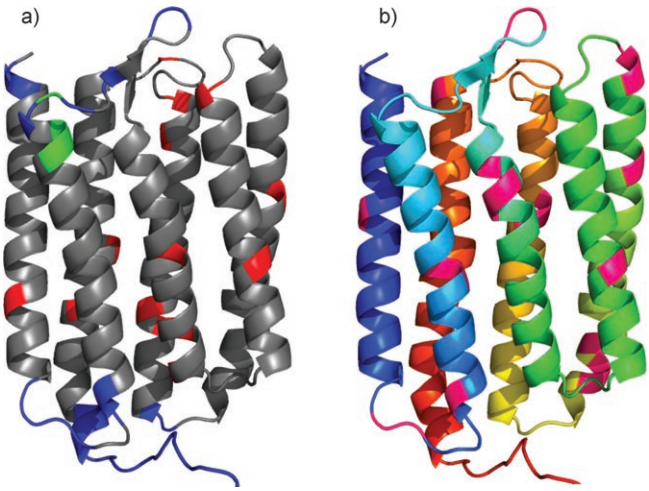


***Figure 5.*** a) Cartoon representations of pSRII based on the crystal structure[13] in (a) showing residues affected by dynamic processes, as monitored by $^{15}$N relaxation. Residues in blue have a heteronuclear NOE $< 0.6$, indicative of motions on the ps–ns timescale, while residues in red exhibit $R_{ex}$ contributions to their transverse relaxation on the μs–ms timescale. Residues that are undergoing dynamics on both timescales are shown in green. In (b), the chemical shifts in our solution study are compared with the solid-state measurements in proteoliposomes;[15] residues with $^{13}$Ca and/or $^{15}$N shift differences exceeding $\pm 1.5$ ppm are shown in magenta. The protein sequence of the protein can be traced in colors changing from blue (N terminus) to red (C terminus).

L5 show increased flexibility, with the HNOE data indicating extensive motion on the ps–ns timescale (Figure 4). Loop L3 does not show any mobility on this timescale, in agreement with the solid-state study. The C-terminal region is confirmed as highly flexible. There are some reduced $T_2$ values, as judged from $R_1 \cdot R_2$ products larger than 20,[26] indicative of the presence of $R_{ex}$ contributions arising from slower fluctuations on the μs–ms timescale. These residues comprise the end of helix B leading into L2, loop L6, and some detergent-exposed residues on the surface of helices A, B, D, E, and F. Interestingly, some inward-facing residues in helices C, E, F, and G are also affected, as shown in Figure 5a. The presence of these $R_{ex}$ contributions for residues within the core of the protein might be indicative of slow interhelix motions, possibly because interactions within the tertiary structure of α-helical membrane proteins are weaker than those in β-barrels.[16]

A comparison between the chemical shifts of backbone residues determined from our solution study in DHPC and those from the solid-state measurements in proteoliposomes should reflect the impact of the different environments on the structure of pSRII. Inevitable uncertainties arise due to the large differences in experimental temperatures and the dissimilar isotope labeling schemes employed. Persisting major differences (Figure 5b) and appear in loops L1, L2, and L6 and on the outward-facing surface of the helices. Residues involved in helix packing are also affected; notably Arg 72 and Ile 74 that precede a small kink in helix C, and Met 145 that follows a Gly–Pro induced kink in helix E. Further differences are seen for Ile 43 and Ser 44 in helix B, and Trp 171 and Ala 172 in helix F. Affected loop regions include a salt bridge between Asp 28 and Arg 34 in L1, residues 64–66 that form part of the β turn in L2, and Thr 189 at the end of L6. Changes observed on the surface and in the loop regions are likely to originate from differences in the thickness of the hydrophobic DHPC phase and when compared with the more nativelike liposome bilayer. Small differences in lateral pressure experienced by the protein in the two media may explain the differences observed for inward-facing residues.[27] Such variations might induce finite changes in the helix packing, with reduced lateral pressures possibly being more permissive of the slow interhelix motions suggested by our $^{15}$N relaxation data. While slow core motions may form part of the native behavior of pSRII, such conformational mobility as observed for some smaller helix-bundle membrane proteins could be a direct consequence of removing the protein from its native bilayer environment.[16,28]

In conclusion, we demonstrate the feasibility of the near-complete backbone assignment (> 98 %) of a detergent-solubilized seven-helical integral membrane protein using solution-state TROSY NMR, and show that the structural integrity of the DHPC-dispersed protein is maintained. The data reported here represent our first step towards a full structure determination of the membrane receptor pSRII in solution. $^{15}$N relaxation data indicate that the helices are well ordered and pack to form a regular helix-bundle. Some of the connecting loop regions are highly flexible and experience motions on the ps–ns timescale, while a limited amount of slow μs–ms helix motion is indicated in the protein core. A basic comparison of chemical shift data with that from a solid-state study in liposomes shows that small variations may arise from the different dimensions of the hydrophobic helix-surrounding media and also indicates the possibility of small changes in interhelix interactions as a result of differences in lateral pressure.

## *Experimental Section*

$^{2}$H,$^{13}$C,$^{15}$N-labeled pSRII was expressed using [$^{2}$H,$^{13}$C]glucose and $^{15}NH_4Cl$ in *E. coli* cells that were stepwise adapted to 100 % $D_2O$. His-tag affinity purification in DM was followed by exchange into DHPC. NMR experiments were performed at 50 °C on Bruker DRX600/800 machines equipped with 5 mm TXI/z probes. TROSY 3D backbone experiments (HNCA, HN(CO)CA, HN(CA)CB, HN(COCA)CB, HNCO, HN(CA)CO) were recorded using nonuniform random sampling schemes, with 256 complex pairs for $^{15}$N and $^{13}$C and an experiment time of approximately six days (total of 1024 combined $^{15}$N,$^{13}$C increments). Sample conditions were approximately 0.5 mM

  

pSRII, pH 5.9, 60 mM DHPC (non-deuterated). Maximum entropy data reconstruction was used in F2 and F3. $^{15}N$ relaxation data were measured at 14.1 T on a $^{2}H,^{15}N$-labeled sample using TROSY-modified sequences. 3D $^{15}N$ NOESY experiments were recorded as HMQC and TROSY versions.

Received: June 12, 2008
Published online: August 1, 2008

**Keywords:** membrane proteins · NMR spectroscopy · protein structures · receptors · structure elucidation

[1] S. H. White, **2006**, Web site: http://blanco.biomol.uci.edu/Membrane_Proteins_xtal.html.
[2] L. K. Tamm, B. Y. Liang, *Prog. Nucl. Magn. Reson. Spectrosc.* **2006**, *48*, 201.
[3] K. R. MacKenzie, J. H. Prestegard, D. M. Engelman, *Science* **1997**, *276*, 131.
[4] M. E. Girvin, V. K. Rastogi, F. Abildgaard, J. L. Markley, R. H. Fillingame, *Biochemistry* **1998**, *37*, 8817.
[5] D. J. Ma, Z. W. Liu, L. Li, P. Tang, Y. Xu, *Biochemistry* **2005**, *44*, 8790.
[6] S. C. Howell, M. F. Mesleh, S. J. Opella, *Biochemistry* **2005**, *44*, 5196.
[7] L. P. Yu, C. H. Sun, D. Y. Song, J. W. Shen, N. Xu, A. Gunasekera, P. J. Hajduk, E. T. Olejniczak, *Biochemistry* **2005**, *44*, 15834.
[8] K. Oxenoid, J. J. Chou, *Proc. Natl. Acad. Sci. USA* **2005**, *102*, 10870.
[9] K. Oxenoid, H. J. Kirn, J. Jacob, F. D. Sonnichsen, C. R. Sanders, *J. Am. Chem. Soc.* **2004**, *126*, 5048.
[10] J. H. Chill, J. M. Louis, C. Miller, A. Bax, *Protein Sci.* **2006**, *15*, 684.
[11] K. A. Baker, C. Tzitzilonis, W. Kwiatkowski, S. Choe, R. Riek, *Nat. Struct. Mol. Biol.* **2007**, *14*, 1089.
[12] M. E. Call, J. R. Schnell, C. Q. Xu, R. A. Lutz, J. J. Chou, K. W. Wucherpfennig, *Cell* **2006**, *127*, 355.
[13] H. Luecke, B. Schobert, J. K. Lanyi, E. N. Spudich, J. L. Spudich, *Science* **2001**, *293*, 1499.
[14] A. Royant, P. Nollert, K. Edman, R. Neutze, E. M. Landau, E. Pebay-Peyroula, J. Navarro, *Proc. Natl. Acad. Sci. USA* **2001**, *98*, 10131.
[15] M. Etzkorn, S. Martell, O. C. Andronesi, K. Seidel, M. Engelhard, M. Baldus, *Angew. Chem.* **2007**, *119*, 463; *Angew. Chem. Int. Ed.* **2007**, *46*, 459.
[16] R. Page, J. Moore, H. Nguyen, M. Sharma, R. Chase, F. Gao, C. Mobley, C. Sanders, L. Ma, F. Sönnichsen, S. Lee, S. Howell, S. Opella, T. Cross, *J. Struct. Funct. Genomics* **2006**, *7*, 51.
[17] K. Pervushin, R. Riek, G. Wider, K. Wuthrich, *Proc. Natl. Acad. Sci. USA* **1997**, *94*, 12366.
[18] K. Shimono, M. Iwamoto, M. Sumi, N. Kamo, *FEBS Lett.* **1997**, *420*, 54.
[19] M. Salzmann, K. Pervushin, G. Wider, H. Senn, K. Wuthrich, *Proc. Natl. Acad. Sci. USA* **1998**, *95*, 13585.
[20] M. Salzmann, G. Wider, K. Pervushin, H. Senn, K. Wuthrich, *J. Am. Chem. Soc.* **1999**, *121*, 844.
[21] J. C. J. Barna, E. D. Laue, *J. Magn. Reson.* **1987**, *75*, 384.
[22] D. Rovnyak, D. P. Frueh, M. Sastry, Z. Y. J. Sun, A. S. Stern, J. C. Hoch, G. Wagner, *J. Magn. Reson.* **2004**, *170*, 15.
[23] T. L. Hwang, A. J. Shaka, *J. Magn. Reson.* **1998**, *135*, 280.
[24] W. J. Metzler, K. L. Constantine, M. S. Friedrichs, A. J. Bell, E. G. Ernst, T. B. Lavoie, L. Mueller, *Biochemistry* **1993**, *32*, 13818.
[25] N. J. Baxter, M. P. Williamson, *J. Biomol. NMR* **1997**, *9*, 359.
[26] J. M. Kneller, M. Lu, C. Bracken, *J. Am. Chem. Soc.* **2002**, *124*, 1852.
[27] A. R. Curran, R. H. Templer, P. J. Booth, *Biochemistry* **1999**, *38*, 9328.
[28] C. R. Sanders, K. Oxenoid, *Biochim. Biophys. Acta Biomembr.* **2000**, *1508*, 129.

  